Meteorol. Atmos. Phys. 49, 69–91 (1992)

Meteorology and Atmospheric Physics



Department of Atmospheric Science, Colorado State University, Fort Collins, U.S.A.

# A Comprehensive Meteorological Modeling System – RAMS

**R. A. Pielke, W. R. Cotton, R. L. Walko, C. J. Tremback, W. A. Lyons, L. D. Grasso, M. E. Nicholls, M. D. Moran, D. A. Wesley, T. J. Lee,** and **J. H. Copeland**

With 18 Figures

Received November 18, 1991
Revised April 16, 1992

**Summary**

This paper presents a range of applications of the Regional Atmospheric Modeling System (RAMS), a comprehensive mesoscale meteorological modeling system. Applications discussed in this paper include large eddy simulations (LES) and simulations of thunderstorms, cumulus fields, mesoscale convective systems, mid-latitude cirrus clouds, winter storms, mechanically- and thermally-forced mesoscale systems, and mesoscale atmospheric dispersion. A summary of current RAMS options is also presented. Improvements to RAMS currently underway include refinements to the cloud radiation, cloud microphysics, cumulus, and surface soil/vegetative parameterization schemes, the parallelization of the code, development of a more versatile visualization capability, and research into meso-$\alpha$-scale cumulus parameterization.

## 1. RAMS Overview

The Regional Atmospheric Modeling System (RAMS) was developed at Colorado State University in order to merge several numerical weather simulation codes being used side by side at the same site (i.e., Pielke, 1974; Tripoli and Cotton, 1982; Tremback et al., 1985). It was concluded that a unified modeling system with the attributes of the original separate models would facilitate more effective scientific research in the Department of Atmospheric Science at Colorado State University. In addition, in the merging of the capabilities of the different models, a range of specific enhancements were introduced to RAMS of which the telescoping, interactive nested-grid capability is one of the most significant. Based on the two-way grid interactive procedures of Clark and Farley (1984), RAMS has the ability to represent a large-scale area (e.g. the Northern Hemisphere) and then to nest progressively to smaller scales (e.g., a $10\,km^3$ volume of the atmosphere). More than one set of telescoping nests can be specified within a larger-scale grid and user-specified, and movable, grids can be activated. RAMS has a non-hydrostatic option so that all meteorologically relevant spatial scales can be represented. The concept of "plug-compatible" modules (e.g., Pielke and Arritt, 1984) is used in RAMS in order to assist developers of parameterizations to interface into RAMS. Plug-compatible means that the interface between the subroutines (i.e., the module) and the rest of RAMS is clearly defined to users of the code.

Current RAMS features and options are shown in Table 1. The use of a FORTRAN preprocessor permits RAMS to be configured easily at run time into one of a wide variety of different models simply by choosing from this table of numerical and physical options. A detailed overview discussion of RAMS and these options is given in Walko and Tremback (1991). The architects of RAMS are Craig J. Tremback and Robert L. Walko, who are supported under research contracts and grants of William R. Cotton and Roger A. Pielke. Significant assistance in developing and testing RAMS

Table 1. *Model Characteristics and Options*

| Category | Available options | References and additional remarks |
|---|---|---|
| Basic equations | • Nonhydrostatic; compressible | Tripoli and Cotton (1980). |
| | • Hydrostatic; anelastic or incompressible | Tremback et al. (1985). |
| Dimensionality | • 1D | |
| | • 2D | |
| | • 3D | |
| Vertical coordinates | • Cartesian | |
| | • Terrain-following $\sigma_z$ | Clark (1977); Tripoli and Cotton (1982). |
| Horizontal coordinates | • Cartesian | |
| | • Stereographic tangent plane | Projection tangent point can be located anywhere on sphere. |
| Grid stagger and structure | • Arakawa C grid, single grid (fixed) | |
| | • Arakawa C grid, multiple nested grids (fixed) | No limit on number of grids; no limit on number of nesting levels; grids can be added/removed during simulation. |
| | • Arakawa C grid, multiple nested grids (movable) | |
| Time differencing | • Leapfrog; time split; 2nd or 4th order spatial accuracy | Leapfrog on long timestep, forward-backward on small timestep; flux conservative form (Tripoli and Cotton, 1982). |
| | • Forward; 2nd or 6th order spatial accuracy | Forward-backward time-split; flux conservative form (Tremback et al., 1987). |
| Turbulence closure | • Smagorinsky deformation K | *Ri* dependence (Tripoli, 1986). |
| | • O'Brien K/Blackadar K | O'Brien first-order K for unstable conditions; Blackadar Local K for stable conditions (McNider and Pielke, 1981). |
| | • Deardorff level 2.5 K | Eddy viscosity is a function of prognostic TKE (Deardorff, 1980). |
| Stable precipitation | • No condensation | |
| | • Condensation | Grid points fully saturated or unsaturated. |
| Cumulus parameterization | • None | |
| | • Modified Kuo | Tremback (1990). |
| Explicit microphysics | • None | |
| | • Warm microphysics | Warm rain conversion and accretion of cloud water ($r_c$) to raindrops ($r_r$); evaporation and sedimentation (Tripoli and Cotton, 1980). |
| | • Ice microphysics – specified nucleation | Warm microphysics plus nucleation of ice crystals ($r_i$), conversion nucleation and accretion of graupel ($r_g$), growth of ice crystals ($r_i$), evaporation, melting and sedimentation (Cotton et al., 1982). |
| | • Ice microphysics – predicted nucleation | Warm microphysics plus above plus nucleation and sink of crystal concentration ($N_i$), conversion and growth of aggregates ($r_a$), melting, evaporation and sedimentation. The nucleation model includes: sorption/deposition; contact nucleation by Brownian collision plus thermophoresis plus diffusiophoresis; and secondary ice crystal production by rime-splinter mechanism (Cotton et al., 1986; Meyers et al., 1991). |
| Radiation | • No radiation | |
| | • Shortwave I | Molecular scattering, absorption of clear air (Yamamoto, 1962), ozone absorption (Lacis and Hansen, 1974) and reflectance, transmittance and absorptance of a cloud layer (Stephens, 1978), clear-cloudy mixed |

Table 1. (*Continued*)

| Category | Available options | References and additional remarks |
|---|---|---|
| | | layer approach (Stephens, 1977). See Chen and Cotton (1983, 1987). |
| | • Shortwave II | Effects of forward Rayleigh scattering (Atwater and Brown, 1974), absorption by water vapor (McDonald, 1960), and terrain slope (Kondrat'yev, 1969). See Mahrer and Pielke (1977). |
| | • Longwave I | Emissivity of a clear atmosphere (Rodgers, 1967), emissivity of cloud layer (Stephens, 1978), and emissivity of "clear and cloudy" mixed layer (Herman and Goody, 1976). See Chen and Cotton (1983, 1987). |
| | • Longwave II | Emissivities of water vapor (Jacobs et al., 1974) and carbon dioxide (Kondrat'yev, 1969) and the computationally efficient technique of Sasamori (1972). See Mahrer and Pielke (1977). |
| Surface layer | • Louis (1979) | Surface roughness specified over land, predicted over water. |
| Lower boundary | • Specified air-surface temperature and moisture differences | |
| | • Diagnosed surface temperature and moisture fluxes based on a prognostic soil model | Tremback and Kessler (1985); McCumber and Pielke (1981). |
| | • Vegetation parameterization | McCumber and Pielke (1981); Avissar and Mahrer (1988); Lee (1992). |
| Upper boundary | • Rigid lid | Nonhydrostatic model only. |
| | • Prognostic surface pressure | Hydrostatic model only. |
| | • Material surface | Hydrostatic model only (Mahrer and Pielke, 1977). |
| | • Gravity-wave radiation condition | Klemp and Durran (1983). |
| | • Optional Rayleigh friction layer | With any of the above conditions (Clark, 1977; Cram, 1990). |
| Lateral boundaries | • Radiative boundary condition I | Orlanski (1976). |
| | • Radiative boundary condition II | Klemp and Wilhelmson (1978a, b). |
| | • Radiative boundary condition III | Klemp and Lilly (1978). |
| | • Radiative boundary condition and MCR | Fixed conditions at Mesoscale Compensation Region (MCR) boundary (Tripoli and Cotton, 1982). |
| | • Large-scale sponge boundary conditions | Synoptic-scale boundary forcing (Perkey and Kreitzberg, 1976). |
| | • Large-scale nudging boundary conditions | Synoptic-scale boundary forcing (Davies, 1983). |
| Initialization | • Horizontally homogeneous (HHI) | |
| | • HHI plus variations to force cloud initiation | |
| | • Variable initialization I | NMC and ECMWF data interpolated directly to model grid. |
| | • Variable initialization II | Isentropic analysis of NMC or ECMWF data and/or upper air soundings and interpolated to model grid (Tremback, 1990). |
| Transport and diffusion | • Lagrangian particle dispersion module | Handles point, line, area or volume sources (McNider, 1981; McNider et al., 1988; Uliasz, 1993). |

has been provided by a number of Colorado State University investigators including Jennifer M. Cram, Michael D. Moran, and Greg J. Tripoli.

The remainder of this paper provides additional detail and examples of applications of RAMS. Section 2 discusses model initialization and analysis. Section 3 describes large eddy simulation use of the model, while thunderstorm simulations are described in section 4. Section 5 presents deep cumulus field modeling results using RAMS and simulations of organized mesoscale convective systems are described in section 6. The simulation of mid-latitude cirrus clouds and winter storms are described in sections 7 and 8, respectively. Physiographically-forced mesoscale system modeling is discussed in section 9. Section 10 describes how RAMS output is applied in the modeling of mesoscale atmospheric dispersion. Finally, the revolutionary advancement in computer capabilities in 1991 are presented in section 11.

## 2. Model Initialization and Analysis

### *2.1 Synoptic Analysis*

RAMS includes the ISentropic ANalysis package (RAMS/ISAN) as Option 4 in the Initialization capability (see Table 1) which performs the data analysis tasks for the initial and boundary conditions for larger-scale runs. Isentropic coordinates were used because they have a number of advantages over other coordinate systems when applied to large-scale data analysis. First, since the synoptic scale flow is, to a first approximation, adiabatic, an objective analysis performed on an isentropic surface will better approximate the interstation variability of the atmospheric fields. Second, isentropes tend to be "packed" in frontal areas, thus providing enhanced resolution along discontinuities. Finally, because isentropes are sloped in the vicinity of fronts, short-wavelength features in Cartesian coordinates are transformed in the isentropic system into longer-wavelength features that can be more accurately analyzed objectively with much less smoothing than with other coordinate systems. A few disadvantages to isentropic coordinates are also present, namely that the vertical resolution decreases as the atmospheric stability decreases (e.g., in the planetary boundary layer) and that the isentropes frequently intersect the ground.

RAMS/ISAN has the ability to combine or blend several data sets in the data analysis and its modular structure simplifies insertion of nonstandard data sets. The code currently supports the NMC mandatory-level 2.5° global-analysis data set, the ECMWF 2.5° global-analysis data set, and NMC rawinsonde and surface observation data sets, all of which are archived at the National Center for Atmospheric Research (NCAR), as standard data sources. All significant and mandatory level wind, temperature, and moisture data can be used from the rawinsonde reports. The capability also exists to input special soundings, bogus soundings, or any additional surface observations that are available. The code is also being initialized with the NOAA Forecast Systems Laboratory MAPS[1] analysis fields.

The data analysis technique can be summarized as follows. The horizontal wind components, pressure, and relative humidity from the gridded global analysis and any available rawinsonde data are interpolated vertically (linearly in $p^{R/c_p}$) to isentropic levels at a user-specified resolution. The Barnes (1973) objective analysis scheme is then applied to these variables on the isentropic surfaces with user-specified parameters in the scheme controlling the amount of smoothing. Once the variables have been objectively analyzed to the analysis grid, the Montgomery streamfunction is then obtained in a hydrostatic integration from an objectively analyzed streamfunction "boundary condition" at an isentropic level near the tropopause. Any horizontal interpolations use the overlapping polynomial technique of Bleck and Haagenson (1968).

The atmospheric variables at the Earth's surface are analyzed in a similar manner to the upper air variables. Wind components, potential temperature, and relative humidity are objectively analyzed. Pressure and Montgomery streamfunction are obtained hydrostatically from the first isentrope above the ground.

Once the isentropic dataset is complete, the atmospheric variables and topography are transferred to the model grid using overlapping polynomial interpolation. First, the wind components, Montgomery streamfunction, and relative humidity are interpolated on the isentropic surface to the model grid point. The height of the isentropic

[1] Mesoscale Analysis and Prediction System.

surface can then be found and the wind, potential temperature, and relative humidity are interpolated linearly in height to the model's $\sigma_z$ coordinate levels. A final hydrostatic integration is done to find the pressure on the model grid.

Although not generally available, soil moisture and temperature data, as well as other soil properties and vegetation characteristics, are also required at the spatial resolution of the model simulations. Techniques to obtain this information represent a major new area of research (e.g., Goodchild et al., 1992).

### *2.2 Four-Dimensional Data Assimilation*

We shall now move from existing analysis and initialization packages to work in progress. Four-dimensional data assimilation (4DDA) involves the effective integration of time-dependent observational data into a predictive model. This can be done during the initial stages of a model run as in Newtonian relaxation (more commonly known as "nudging") or in a variational scheme like the adjoint method. Each of these techniques is discussed below.

#### 2.2.1 Nudging

In the nudging scheme an extra tendency term is added to each prognostic equation which forces the predicted variable towards the available observations.

$$\frac{\partial x}{\partial t} = F(x) + N(x, y, z, t)\cdot(x_0 - x) \tag{1}$$

Here $x$ is a model variable, $F(x)$ is the model's physics, $N(x, y, z, t)$ is the nudging weight, and $x_0$ the observation of the model variable (Wang and Warner, 1988).

There has been limited success with nudging toward a gridded analysis and to the observations themselves on the meso-$\alpha$ scale, where data separations of 400 km exist (Stauffer and Seaman, 1990). Walko et al. (1989) showed, using hypothetical radar-derived winds, that nudging with incomplete data (not the full set of predictive variables) may or may not improve the model prediction. In fact in some cases the prediction was degraded by the 4DDA scheme. The current setup of RAMS has the capability for 4DDA via the nudging method.

#### 2.2.2 Adjoint Method

Recent advances in 4DDA, based on optimal control theory, hold promise for assimilating four-dimensional observations into a dynamically consistent initial condition. New to the atmospheric community, this approach is called the adjoint method. The adjoint method is essentially a mathematical tool for obtaining the gradient of a real-valued function, in the case of 4DDA, a prognostic model. The following variational approach for the assimilation of observations is under development: *Define a real-valued function ($\mathcal{J}$) measuring the "distance" between the model solution corresponding to a given initialization ($\bar{x}_0$) and the available observations* (Taylor, 1991). Then, using the adjoint method, the gradient of this distance function with respect to the initial condition can be calculated ($\nabla\mathcal{J}_{\bar{x}_0}$). Using a gradient-based minimization algorithm (Buckley, 1985), that initialization for which the distance is a minimum is calculated via an iterative process. This procedure is illustrated in Fig. 1. Thus, using this initialization the model will predict values that most closely fit the known observational data.

For the mathematical theory behind the derivation of the adjoint model, we refer the reader to the following papers: Lewis and Derber (1985), Talagrand and Courtier (1987), Thacker and Long (1988), Courtier and Talagrand (1990), and Copeland et al. (1991).

The advantage of this method over nudging is the dynamic consistency of the initial conditions and the scheme's ability to retrieve unmeasured

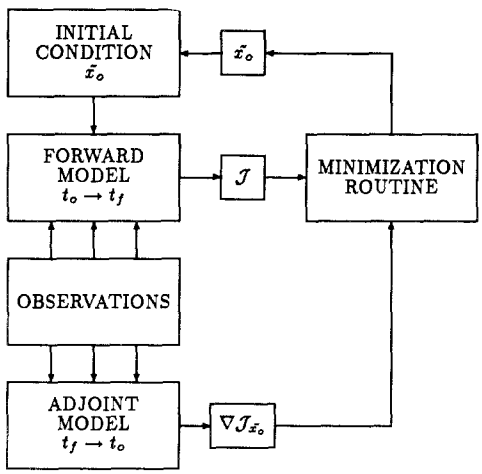


Fig. 1. Schematic of the iteration process for the adjoint method of 4DDA

variables or to utilize observations which are integral properties of model variables (e.g., radar reflectivity). It should also be noted that this method is not limited to simply initializing models. It is quite general and could be used, for example, for determining boundary conditions and also parameterizations. In addition, this method holds great promise as a sensitivity analysis tool. We are currently working on adjoint models of RAMS for 4DDA and diagnostic studies (Verlinde, 1992).

## 3. Using RAMS in an LES Mode

The phrase "large eddy simulation" (LES) is becoming a more popular descriptor of high resolution numerical simulations, no doubt owing in part to the increasing availability of powerful computers to perform them. The term is sometimes used rather loosely, however, to refer to simulations performed on computational grids having a particularly large number of mesh points, but which are otherwise no different from "conventional" simulations. A more useful "LES" definition requires that (1) the computational mesh is fine enough to resolve scales smaller than those of primary interest in the simulation, so that the subgrid parameterization does not have a strong, direct impact on the scales of interest, and (2) the resolved model fields are passed through an appropriate space and/or time filter as a post-processing step to extract the scales of interest. The type of filter depends on the specific information sought from the simulation, and many possibilities exist. The most commonly applied filter in LES of the atmosphere has been a horizontal (and time) average spanning the computational domain, thus yielding mean vertical profiles, such as in studies of the convective boundary layer (CBL) over homogeneous surfaces (e.g., Moeng and Wyngaard, 1984).

Recently, RAMS has been applied in LES of the CBL over non-homogeneous surfaces (using the subgrid parameterization described in Deardorff, 1980). One such application focused on the effect of spatial variations in the surface heat flux on the mean eddy statistics of the boundary layer (Hadfield et al., 1991). Another examined the influence of hilly terrain on the eddy statistics (Walko et al., 1992). An aim of both studies was to see if the mean horizontal statistics differed from those over homogeneous surfaces, and for that purpose, horizontal averaging across the domain combined with time averaging was performed to extract vertical profiles from model fields. Both studies produced the result that the mean profiles based on horizontal averages are essentially identical over the homogeneous and non-homogeneous surfaces applied in those studies.

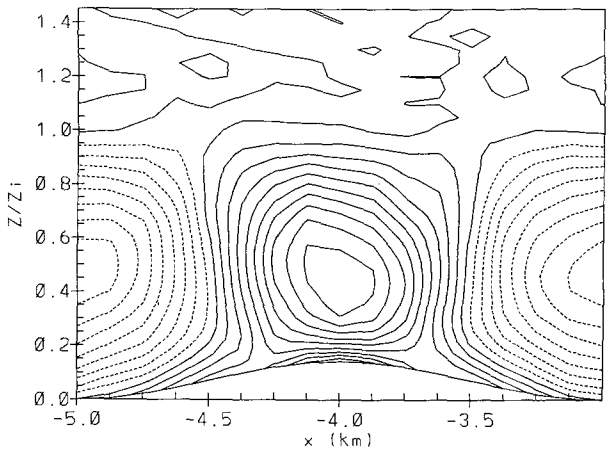


Fig. 2. Cross section of mean vertical velocity over a single hill-valley cycle as a function of normalized height $z/z_i$ and $x$ (in km). The contour interval is 0.04 $w_*$, with dashed lines indicating negative values. The sinusoidal terrain height appears in correct vertical scale in the lower part of the plot (from Walko et al., 1992)

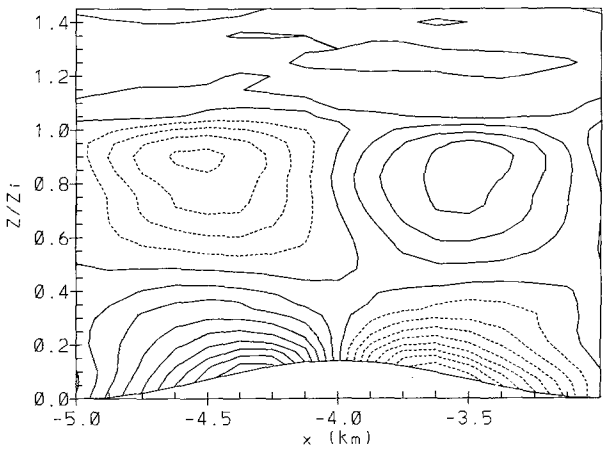


Fig. 3. As in Fig. 2 but for horizontal velocity (from Walko et al., 1992)

Significant differences exist, however, between the eddy fields over homogeneous and variable surfaces. The fact becomes apparent from applying filters other than the full horizontal average described above. For example, Walko et al. (1992)

simulated the CBL over a series of parallel ridges and valleys, and applied a filter which averaged all hill and valley cycles into a single cycle, also averaging in time. Plots of vertical and horizontal velocity extracted from the eddy motions by this filter are shown in Figs. 2 and 3. A mean circulation is evident with subsidence over the valleys, ascending motion over the ridges, upslope flow near the surface, and return flow aloft. The motions account for a significant fraction of the total eddy kinetic energy. Such mean motions, which are induced by the topography, are totally absent from the eddy motions which develop over a homogeneous surface.

There are many other useful LES applications for which different types of filters are needed. For example, RAMS is currently being used to simulate a field of convective clouds on a grid which resolves the primary vertical motions in the clouds. Through proper filtering, the mean vertical redistribution of heat and moisture resulting from the convection under different environmental conditions are determined. These motions will also significantly influence the vertical dispersion of pollutants – an effect that has been largely ignored in air quality studies. This information is being used to develop cumulus parameterization schemes designed for grids with horizontal spacing in the range from 2–20 km (Weissbluth, 1991), where many existing cumulus parameterization schemes are not applicable (e.g., Cram et al., 1992b). The post-processing filter applied to the resolved cumulus field includes conditional sampling of storm updrafts and downdrafts. Specialized filters for this and other applications are being developed in RAMS.

## 4. Thunderstorms

RAMS includes an outgrowth of a cloud model that has been used to simulate thunderstorms (Tripoli and Cotton, 1980; 1986). A recent example of the application of RAMS to simulating thunderstorms is the simulation of the Del City 20 May 1977 tornadic thunderstorm performed by Louie Grasso as part of his M.S. thesis (Grasso, 1992). Using the interactive, nested-grid configuration, RAMS was set up with a coarse grid having 1 km spacing in the horizontal directions over a 40 km × 40 km domain in the horizontal and 16 km in the vertical. The vertical grid increment was stretched from 25 m near the ground to 666 m with a 1.2 stretch ratio.

The model was initialized with a horizontally homogeneous composite sounding taken on 20 May 1977 at 1500 CST at Fort Sill, Oklahoma and 1620 CST at Elmore City, Oklahoma. The Klemp–Wilhelmson (1978a) radiative lateral boundary condition was used along with a wave-absorbing layer in the top-most seven levels. Two additional grids were spawned after 90 minutes of simulation: Grid 2 was one-third the size of Grid 1 and had 333 m horizontal spacing while Grid 3 was one-third the size of Grid 2 and had 111 m horizontal grid spacing.

After triggering the storm with a warm cube of dimensions 10 km × 10 km × 3 km which was 1.5 °C warmer and 2 g kg$^{-1}$ moister than its environment, a steady, rotating supercell storm formed which exhibited all the major features of a supercell storm, including strong, steady updrafts and downdrafts, rotation in the updrafts, a well-defined bounded weak echo region, and a hook echo including a V-notch. Figure 4 illustrates an updraft core that extends to about 14 km AGL with peak speeds on the order of 45 m s$^{-1}$. The surface precipitation field shown in Fig. 5 exemplifies the simulated storm structure, including precipitation rates over 54 mm hr$^{-1}$, the well-defined hook echo and V-notch, a maximum of precipitation located near the V-notch, and a secondary maximum located some 20 km to the northeast.

On Grid 3, a tornadic circulation developed that exhibited a maximum updraft at 12 m AGL of 8.4 m s$^{-1}$ with a dimension of 500 m and pressure deficit of 12.8 mb. At 365 m AGL the tornadic updraft increased in strength to a magnitude of

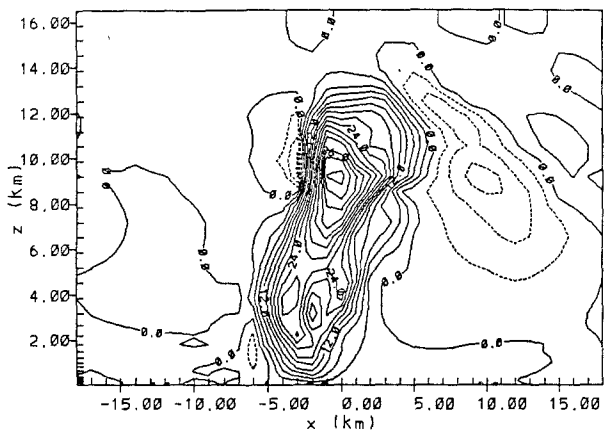


Fig. 4. Vertical cross section of the vertical motion at $y = -1$ km on Grid 1 at 95 min into the tornado simulation (from Grasso, 1992)

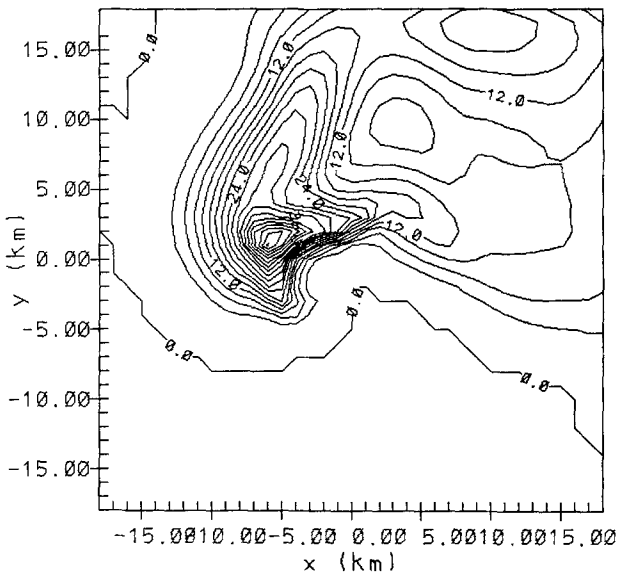


Fig. 5. Total ground precipitation of Grid 1 with horizontal resolution of one kilometer at 103 min into the simulation. Contours are every 2 mm $hr^{-1}$. The maximum precipitation is 54 mm $hr^{-1}$ (from Cotton, 1991)

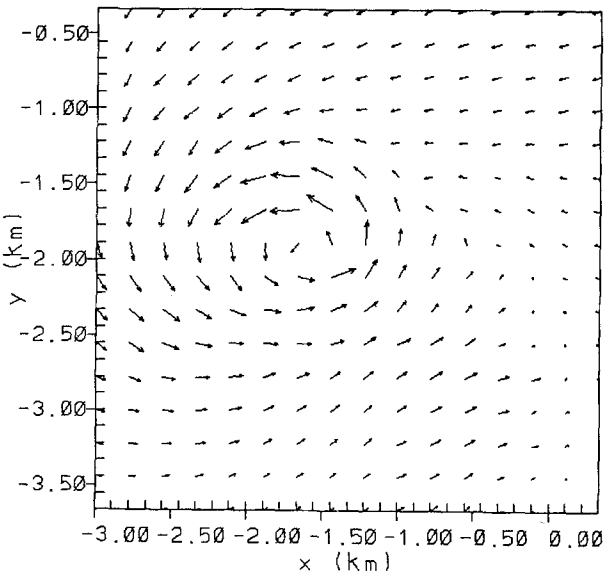


Fig. 6. Horizontal wind vectors at 365 m AGL and 105 min into the simulation for Grid 3. The largest vector is 50 $ms^{-1}$ (from Cotton, 1991)

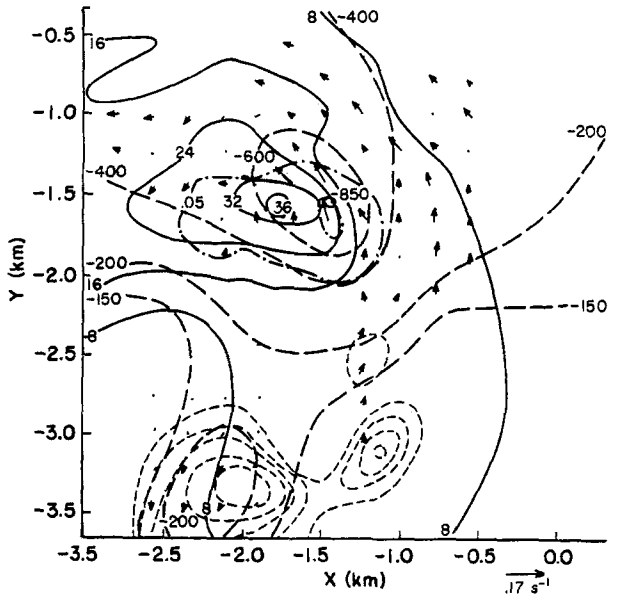


Fig. 7. Horizontal cross section at 1095 m AGL and 96 min into the simulation for Grid 3. Updraft speed is indicated by solid lines, perturbation pressure by long dashed lines, positive vertical vorticity by dashed-dot lines, negative vertical vorticity by short dashed lines, and the arrows represent horizontal vorticity vectors (from Grasso, 1992)

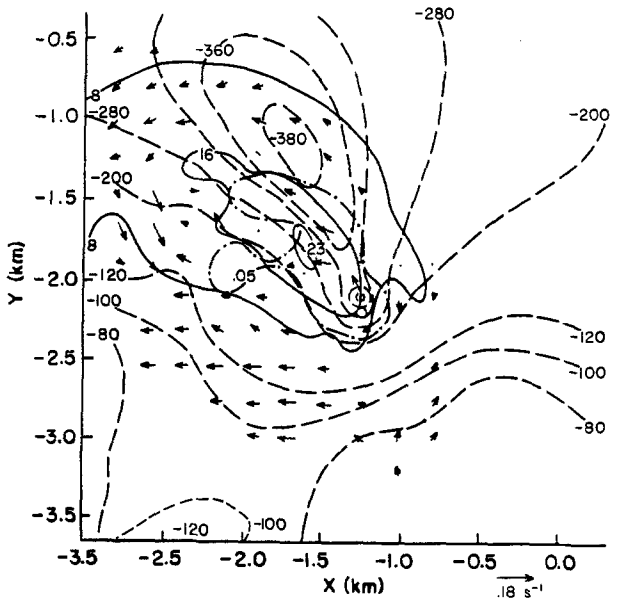


Fig. 8. Same as Fig. 7 except at 463 m AGL (from Grasso, 1992)

60 m $s^{-1}$ with a 30 mb pressure drop. Maximum tangential wind speeds ranged from 45 m $s^{-1}$ at 111 m AGL to over 50 m $s^{-1}$ at 365 m AGL. Figure 6 illustrates the closed circulation of the tornadic vortex at the 365 m level.

Figure 7 illustrates the simulated updraft speed, perturbation pressure, positive vertical vorticity, negative vertical vorticity, and horizontal vorticity vectors near cloud base (1095 m AGL) at 96 min into the simulation. Note that the largest pressure deficit and maximum vorticity are co-located with the strongest gradient in updraft speeds. As illustrated in Fig. 8, the maximum vorticity is still

located in the region of the strong updraft velocity gradient and this is a consistent feature throughout the depth of the tornado.

The mechanisms responsible for the formation of the simulated tornado have been investigated in detail by Grasso (1992). It appears that the tornadic circulation develops in response to localized pressure falls in the region of strong updraft gradient in the mesocyclone. The falling pressure produces an upward-directed pressure gradient, which increases the updraft strength at lower levels and the associated updraft gradient. Pressure falls at the lower levels, and leads to enhanced vorticity and successive downward propagation of the vortex. The tornadic vortex thus builds downward along the updraft gradient channel. This process cannot proceed to the ground, however, because strong updraft gradients are not possible near the ground and tilting of vortex tubes is inhibited. The simulation shows that a cyclonic circulation near the ground is produced as the downdraft from the precipitation region to the northwest of the updraft rotates cyclonically around the rear side of the storm, the leading edge of which is the gust front. Convergence in the low-level accelerating updraft air therefore strengthens and draws in sub-cloud air rich in cyclonic vorticity. The enhancement of sub-cloud cyclonic vorticity allows the pressures to fall and a vertically coherent tornadic vortex forms.

This simulation illustrates just how robust RAMS is in simulating very tight gradients and intense circulations using interactive, nesting procedures.

## 5. Cumulus Field Results

An important aspect of cloud dynamics is the upscale development from shallow cumulus to deep convection. Over the Florida peninsula a common occurrence is the development of numerous cumulus at midday prior to the onset of deep convection. Two-dimensional simulations of this upscale development are presented by Nicholls et al. (1991). In the simulations, surface heating during the morning resulted in the generation of sea breezes. Organized uplift developed at the sea-breeze fronts, but once the convective temperature was reached, Rayleigh-Bernard instability in the, as of yet, unsaturated atmosphere resulted in the formation of numerous convective cells in

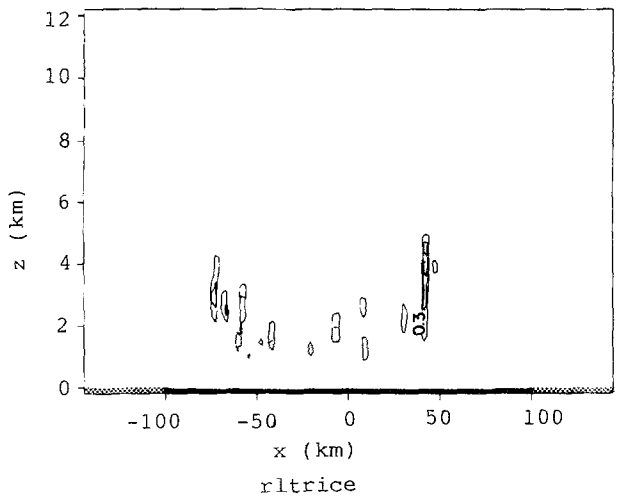


Fig. 9. Simulated cloud-water field at 1300 EST. The contour interval is $0.3\,g\,kg^{-1}$. The thick solid line at the surface, between $x = -100$ km and $x = 100$ km, represents the peninsula; the remaining region is the sea (from Nicholls et al., 1991)

between the fronts. As these cells became deeper, the lifting condensation level was reached, producing a shallow cumulus field extending across the peninsula. Figure 9 shows the total liquid and ice water field at 1300 EST for one simulation which began at 0800 EST. The deepest cells occur at the sea-breeze fronts with shallower cells in between. The cells that develop over the peninsula produce strong upward eddy transports of sensible heat and moisture. The deeper outer cells appeared to enhance the propagation speed of the sea-breeze fronts due to evaporational cooling and water loading which increased the pressure gradient across the fronts. As these outer cells grew deeper, compensation subsidence apparently resulted in the suppression of the smaller-scale cells in between the fronts. These initial deep cells were typically left behind by the more rapidly moving sea-breeze fronts which converged in the afternoon, resulting in explosive deep, moist convective development over the middle of the peninsula. For these simulations, the shallow convection that developed in between the sea-breeze fronts had only a modest influence on the later development of strong convection. The low-level convergence of the oppositely moving sea breezes seemed to be the most dominant control for determining the timing and location of the strongest convective development.

Experiments were performed for different soil moistures. For the moist soil case, the sensible

heat flux was reduced, resulting in a weaker sea-breeze circulation. Numerous shallow clouds formed in between the sea-breeze fronts after mid-day. For the dry soil case, stronger surface heat fluxes resulted in more rapidly moving sea-breeze fronts producing explosive deep moist convective development earlier in the afternoon. Even though the low-level moisture available for convection was less for this case, the stronger low-level convergence produced convection which was as intense as for the moist soil case.

Preliminary three-dimensional multiple nested grid simulations of Florida convection have also been made with RAMS. Previous sea-breeze simulations, typically with mesh sizes on the order of 10 km, realistically resolved Florida's east and west coast sea-breeze convection. Yet in the vicinity of the Kennedy Space Center the coastline is complex, with several large islands (Merritt Island and Cape Canaveral) separated from the mainland by 5–10 km wide estuaries. The islands develop their own localized "heated island" circulations embedded within the larger sea-breeze regime. These vertical motion patterns only become resolved as the model mesh size is reduced to 3 km or less. Thus, the resolved mesoscale flows can be both qualitatively and quantitatively dependent upon the selected mesh size. A climatology reveals that a "Merritt Island Thunderstorm" (MIT), distinct from Atlantic sea-breeze thunderstorms, develops on 15% of summer days during mid-morning due to the localized island heating. RAMS simulated an MIT, using explicit microphysics and a 1000 m mesh, with considerable fidelity in a three-dimensional configuration (Lyons et al., 1992). Two-dimensional simulations failed to properly resolve the island-induced flows and convection.

## 6. Mesoscale Convective Systems

One of the applications of RAMS has been the simulation of mesoscale convective systems (MCSs). MCSs have a horizontal scale of several hundred kilometers or so and are composed of a number of thunderstorm cells. Sometimes the cells exhibit well-defined organization such as squall lines while others exhibit seemingly random organization of cells. MCSs are a challenge to modelers because they are of a large horizontal scale and have such long lifetimes yet are strongly dependent upon smaller-scale motions associated with cumulonimbus clouds. As a result, simulation of MCSs involves considerable compromise.

For example, in our earlier work as well as that of many other groups, MCSs have been simulated in two dimensions. These studies include the influence of radiation and ice-phase microphysics on the dynamics of stratiform-anvil clouds (Chen and Cotton, 1988), the influence of stratification and deep tropospheric shear on derecho-producing squall lines (Schmidt and Cotton, 1990), tropical squall line maintenance and structure (Nicholls et al., 1988), and the genesis of mesoscale convective systems over the Colorado Rockies (Tripoli and Cotton, 1989a, b). Each of these simulations were limited by the fact that both the convective storms and the mesoscale circulations were represented in two dimensions. Even for two-dimensional squall lines which have a pronounced two-dimensional appearance, the thunderstorms embedded in the line are not well represented in two dimensions. Moreover, the longer-lived squall lines and other MCSs undergo significant geostrophic adjustment and thereby develop flow structures which are clearly three-dimensional.

The other compromise that has been made is to simulate MCSs with coarse horizontal resolution and implement a cumulus parameterization scheme to simulate the smaller-scale cloud processes. In general these simulations are initialized from an objectively-analyzed, spatially-variable synoptic field. Tremback (1990) was the first to use RAMS in this mode of operation. Using the hydrostatic version of RAMS with both 80 km and a 45 km grid-point separation, he simulated the initiation and propagation of a squall-line-like mesoscale convective complex (MCC) over the northern High Plains. This simulated storm was initiated by a regional-scale mountain/plains solenoidal circulation and subsequently propagated slowly eastward with the solenoid (at $\sim 12$–$14\,\mathrm{m\,s^{-1}}$) and then propagated (at $\sim 22\,\mathrm{m\,s^{-1}}$) as a fast-moving gravity wave disturbance. The model simulated the observed gross behavior of the MCC quite well but did not represent more ordinary cumulonimbus clouds over Colorado and the central High Plains correctly. The results of this simulation were very sensitive to the specification of the initial soil moisture field and to the detailed formulation of the convective parameterization scheme. This is unfortunate since we have difficulty obtaining access to regional soil moisture data, and we have

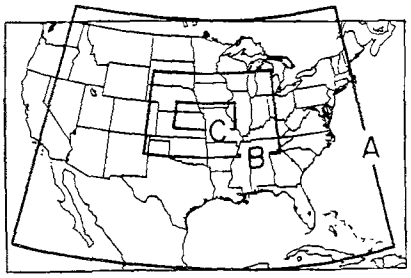


Fig. 10. Domains of 80 km, 20 km, and 5 km grids. Domain boxes are labeled A, B, and C, respectively (from Cram et al., 1992b)

little confidence in the quantitative value of convective parameterization schemes when applied to mesoscale models. It is interesting to note that Schmidt (1991) repeated Tremback's simulation, but with the non-hydrostatic version of RAMS and using interactive grid nesting with the finest grid having 25 km grid spacing. He found little difference between the two solutions, suggesting that the meso-$\alpha$-scale features of such a system can be simulated well with a hydrostatic model.

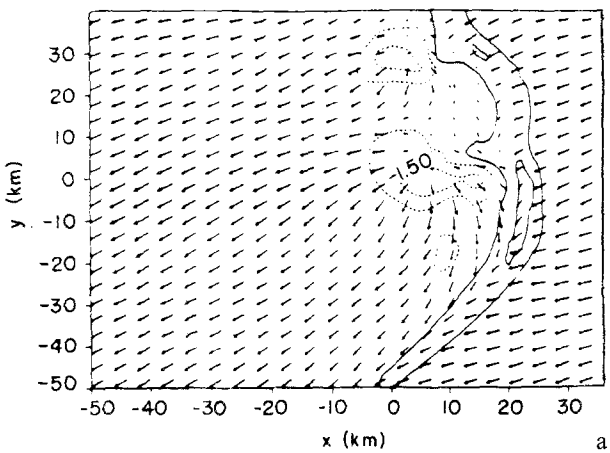


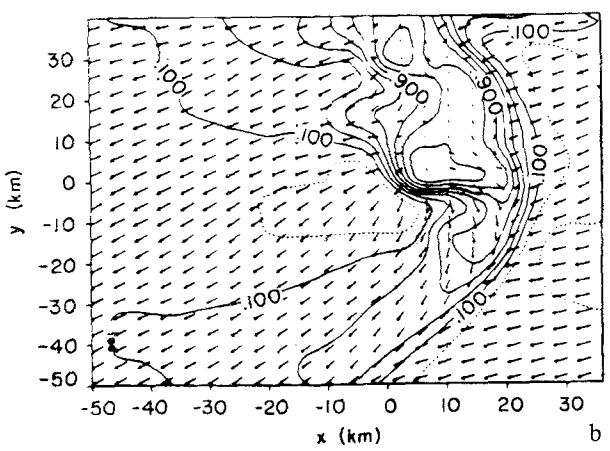


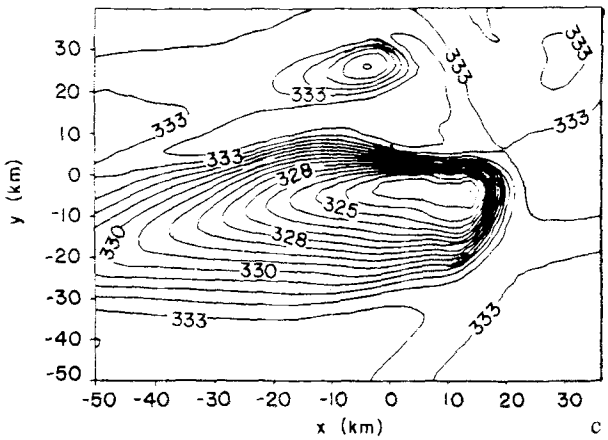


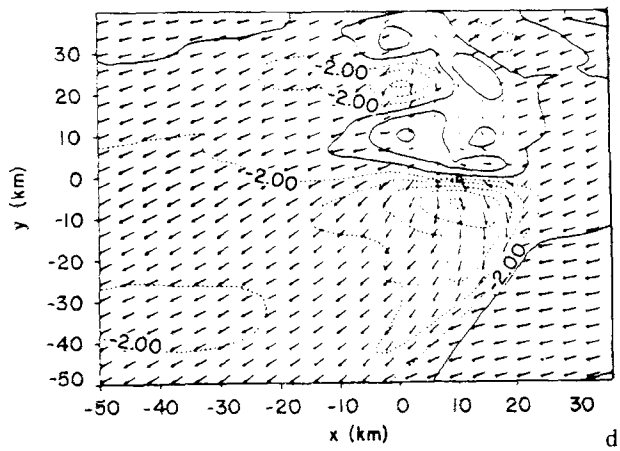


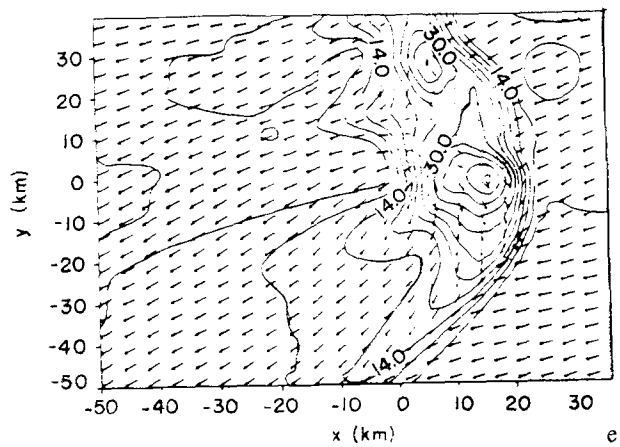


Fig. 11. Horizontal $x$-$y$ cross-sections of the near surface ($z = 146$ m) fields for the curved hodograph experiment at 10800 s. The fields shown are (a) storm-relative flow vectors and vertical motion $w$ contoured every 1 m s$^{-1}$, (b) storm-relative flow vectors and perturbation Exner function $\pi'$ contoured every 0.2 J kg$^{-1}$ K$^{-1}$, (c) equivalent potential temperature $\theta_e$, (d) storm-relative flow vectors and $u'$ contoured every 4 m s$^{-1}$, and (e) storm-relative flow vectors and $v'$ contoured every 4 m s$^{-1}$. Solid lines denote positive values of contoured variable in each panel (from Schmidt, 1991)

In another example of an inhomogeneous initialization of an MCS with RAMS, Cram (1990) and Cram et al. (1992a, b) simulated a large pre-frontal squall line. In this case RAMS was set up non-hydrostatically with three interactive grid nests with grid spacings of 80 km, 20 km, and 5 km, respectively (see Fig. 10). On the two coarser grids, a Kuo-type cumulus parameterization was used. The model responded by producing a fast-moving pre-frontal squall line similar to the observed system which propagated at the speed of an internal gravity wave. However, when the five-kilometer grid spacing domain was activated without a convective parameterization scheme, a pre-frontal line was not simulated. The introduction of enhanced vertical diffusion only produced convection along the frontal boundary. These results further showed the importance of a convective parameterization scheme even on models with grid point separation as small as 5 km. Hopefully, a new scheme developed by Weissbluth (1991) will solve this problem.

Finally, a third compromise one can make in simulating smaller MCSs is to initialize with just a single sounding in three dimensions and then simulate a MCS from a prescribed initial perturbation such as a low-level cooling function or a hot bubble. Schmidt (1991) used this approach to examine the processes responsible for severe derecho wind formation in a bow-shaped squall-line. As shown in Fig. 11, this approach can produce realistic-looking squall-line features for lines having a long dimension on the order of 100 km and lifetimes of 3 or 4 hours. For squall lines of much longer durations or larger dimensions, however, horizontally-inhomogeneous initialization procedures are needed.

## 7. Simulation of Mid-Latitude Cirrus Clouds

The simulation of mid-latitude cirrus clouds represents a somewhat different application of RAMS. Most other applications are strongly dependent upon surface forcing either as it impacts boundary-layer flows and transport and diffusion or generates orographic and convective clouds. In the case of cirrus clouds, the primary forcing arises from synoptic-scale motions associated with extra-tropical cyclones and jet streaks which produce slow, slantwise ascent of moist air. In response to these large-scale motions, gravity waves, radiative-convective forcing, and condensation/evaporation

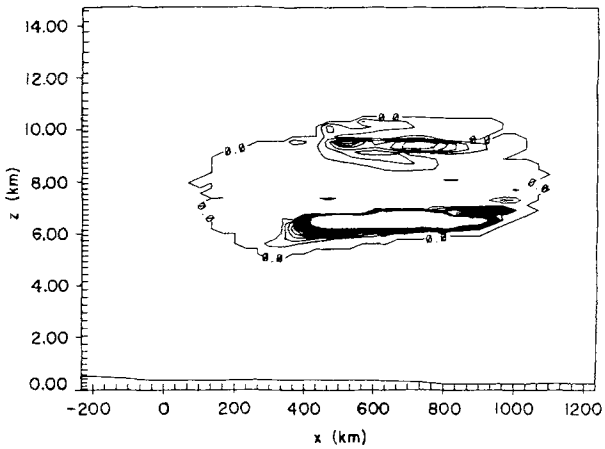


Fig. 12. Vertical cross section at $j = 25$ on the nested grid for 1500 UTC of crystal concentration (crystals/liter) (from Heckman, 1991)

of precipitation particles can produce smaller-scale structures in the cloud systems. As a result, the simulation of cirrus clouds places a greater burden on the RAMS/ISAN package for capturing and depicting the large-scale motions correctly.

Recently, Heckman (1991) simulated cirrus clouds observed during the 28 October 1986 FIRE I case study. He set up the three-dimensional, non-hydrostatic version of RAMS on two nests, the outer grid having 100 km horizontal grid spacing and the fine grid having 33 km spacing. In order to resolve the vertical structure of cirrus clouds he used 69 vertical levels with 200 m vertical grid-point spacing between 5 km and 11 km MSL. One adverse impact of selecting so many vertical levels arises because the longwave radiation scheme developed by Chen and Cotton (1983) uses an effective emissivity approximation in which the number of calculations is proportional to the number of levels squared. As a result this radiation scheme consumed 70% of the computer resources in the RAMS simulation in spite of the fact that the scheme was only activated at 15 minute intervals!

In this particular case RAMS did an excellent job of replicating the observed cirrus cloud coverage and the time evolution of the cloud field. In addition, as shown in Fig. 12, the model was able to reproduce the observed layered structure of the cirrus clouds. The results of this study are encouraging but represent only a single case study. Many more cases are required to determine how effective RAMS is in simulating the full extent of conditions leading to cirrus cloud formation.

## 8. Winter Storms Simulations

Numerical investigations of the effects of topography on winter storms have been undertaken over the last several years using RAMS (Wesley et al., 1990, Wesley, 1991; Meyers and Cotton, 1992). The studies included extensive simulations utilizing the two- and three-dimensional, non-hydrostatic nested versions of the model. The simulations emphasized terrain effects both in the Sierra Nevada and the Front Range of the Rocky Mountains. Most of this section will describe a series of runs designed to augment the detailed observational case study of the 30–31 March 1988 heavy snowstorm which occurred over the northern Front Range of Colorado. Snow was especially heavy over the foothills and adjacent plains (see the snowfall distribution in Fig. 13 and Wesley and Pielke, 1990).

The simulation utilized silhouette-averaged topography (Bossert, 1990) in order to incorporate the desired terrain effects. Horizontal grid spacings were approximately 22 km and 100 km for the fine and coarse grids, respectively. Vertical spacing was stretched from 100 m at the surface to 500 m above 9 km. The coarse grid covered the western and central U.S., southern Canada, eastern Pacific Ocean, and northern Mexico. The inner grid was centered over the northern Front Range of Colorado. The model initialization consisted of the ISAN analysis of NMC gridded data at mandatory levels, along with standard radiosonde and surface observations across the coarse domain.

The model was run with one grid for four hours, at which time the second grid was added. Detailed microphysics, including calculations of mixing ratios of aggregates, graupel, and rain, as well as precipitation of these species, were incorporated into the simulations after six hours. Figure 14 shows the accumulated liquid equivalent of precipitation predicted by the model after 24 hours of simulation, or 18 hours with detailed microphysics, for the fine grid. As shown, the model captured the development of heavy precipitation, the majority of which consisted of aggregates, over the elevated terrain in northern Colorada and Wyoming with a maximum accumulation of approximately 35 mm. The precipitation development was primarily the response to the strong low-level upslope (easterly) flow in this region. Some underprediction of snowfall east of the foothills was

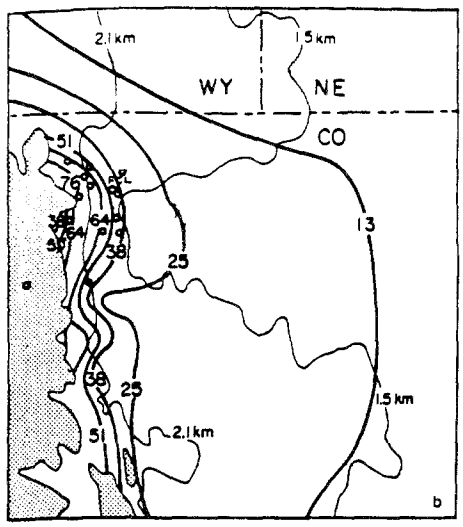


Fig. 13. Snowfall distribution (cm) along the northern Colorado Front Range for 30–31March 1988. Elevation contours (km) are the thin lines. Elevations above 2.7 km are shaded. NWS station identifiers are as follows: Laramie (LAR), Cheyenne (CYS), Sidney (SNY), Akron (AKO), Fort Collins (FCL), Limon (LIC), Denver (DEN), Colorado Springs (COS), and Christman Field (CHR). State borders are the dotted lines. The capital letters A and B refer to the Cheyenne Ridge and Palmer Divide, respectively. Secondary locations mentioned in the text are Akron (AKO), Boulder (B), Limon (LIC), Vail (V), Estes Park (E), Glenwood Springs (G), Rifle (1V1), Leadville (LXV), and Winter Park (W) (from Wesley, 1991)

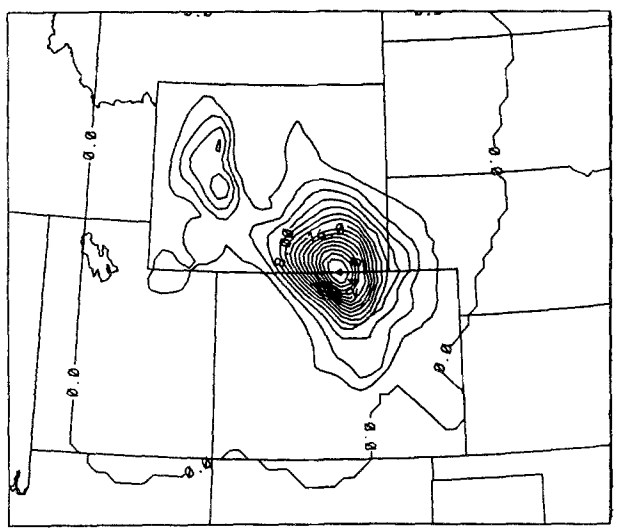

Fig. 14. Total model-predicted accumulated liquid precipitation (mm) for 18 hours of simulation with microphysics activated ending at 1200 GMT 31 March 1988 (from Wesley, 1991)

evident upon comparison to Fig. 13. This problem was attributed to both insufficient horizontal resolution in the fine grid and to the size of the fine-grid domain.

For snowstorms involving Arctic outbreaks along the Colorado Front Range, several two-dimensional experiments using RAMS have examined the dynamics associated with a trapped cold air mass. The presence of this Arctic air mass essentially alters the effects of the lee-side topography on the prevailing westerly flow aloft, a conclusion that was also reached in Lee et al. (1989). The magnitude of the downward portion of the terrain-induced mountain wave was reduced by a factor of two when the low-level cold air mass was included in the model initialization. The RAMS predictions also included some deepening of the cold air mass over and adjacent to the foothills, a feature documented previously in satellite images and sounding data (Wesley et al., 1990). These two phenomena can exert a strong influence on the vertical motion fields associated with cold outbreaks, sometimes creating favorable conditions for snow production over the foothills and plains during westerly flow aloft.

Future applications of RAMS will include modification of the fine-grid resolution and domain size in order to successfully capture the essential blocking characteristics of the 30–31 March 1988 storm. Also, a set of three-dimensional numerical experiments designed to investigate the development of the Front Range barrier jet is underway. Currently, the details of the dynamics of this feature, and more importantly its effects on microphysical processes, are largely unclear. The Winter Icing and Storms Project (WISP) (Rasmussen and Politovich, 1990) collected a detailed data set for an excellent barrier jet case, the 5–7 March 1990 blizzard, and this storm is currently being studied using RAMS.

The RAMS microphysical parameterization are currently being upgraded as well. Meyers et al. (1992) implemented several improvements in the microphysical module of RAMS. These include a dependence of condensation freezing and deposition freezing on supersaturation as opposed to solely temperature. For contact nucleation, an improved prediction of potential ice nuclei based on laboratory measurements has been implemented. Furthermore, a scheme currently in development will predict both concentrations and size distributions of all hydrometeor species.

## 9. Physiographically-Forced Mesoscale Systems

The atmosphere has only one natural boundary, namely the Earth's surface, where the atmosphere

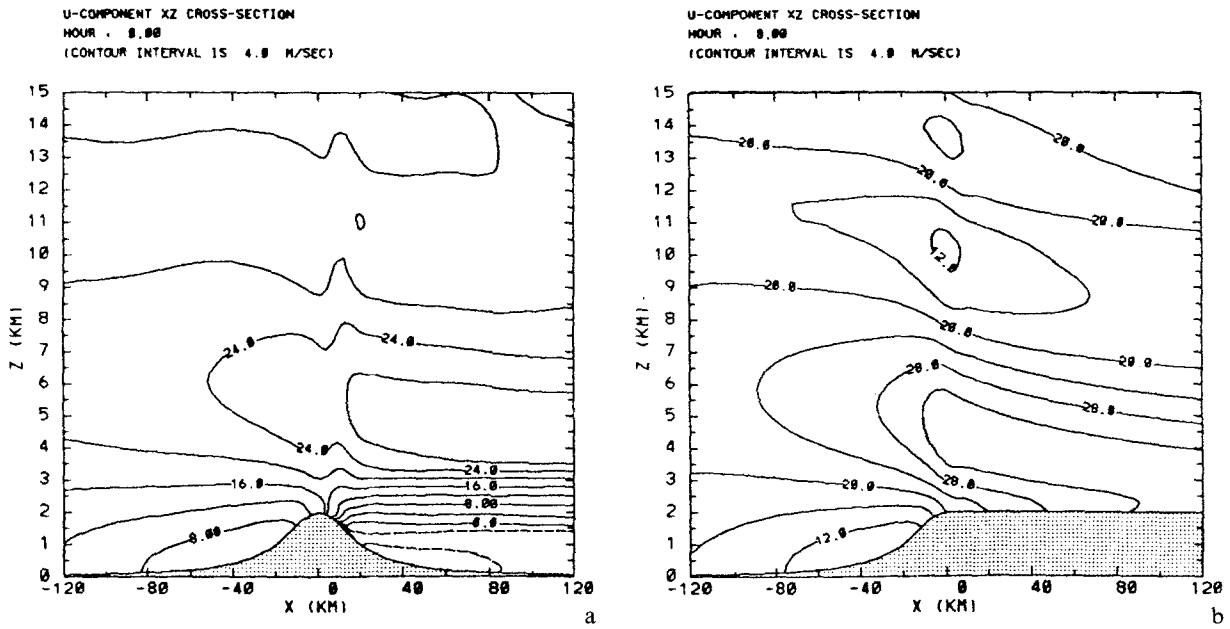


Fig. 15. Cross mountain wind speeds for (a) a bell-shaped mountain with lee-side cold pool, (b) same as (a) but the cold pool is replaced by a plateau with similar shape (from Lee et al., 1989)

exchanges momentum and energy with the Earth. Two types of mesoscale atmospheric circulations are constantly generated by the interaction between the atmosphere and the Earth. The first type is a "mechanically forced circulation" which includes standing mountain waves, propagating lee waves, and upstream blocking events. This type of atmospheric circulation is generated mainly due to the interaction between the stably stratified atmospheric flow and topographic obstacles. Severe downslope wind storms and winter upslope snow storms can develop associated with breaking mountain waves and upstream blocking events, respectively. Using an earlier version of RAMS, Lee et al. (1989) studied the interaction between standing mountain waves and lee-side cold pools. It was concluded that the cold pool can act just like an elevated terrain due to the strong stability and that the downslope wind cannot penetrate the dammed cold air to reach the ground. Figure 15 shows a comparison between two simulations with and without the presence of a cold pool. Extending this result, Wesley (1991) simulated severe winter snow events east of the Colorado Rocky Mountains, as summarized in Section 8. In these examples, RAMS was able to simulate the dynamics of atmospheric flow in response to the terrain forcing, resulting in good replication of wind and precipitation intensities.

The second type of circulation is a "thermally-forced circulation" which includes sea breezes, mountain-valley winds, and other mesoscale circulations due to spatial variations in landscape (e.g., snow breeze, forest breeze). This type of atmospheric circulation is generated mainly due to differential surface heating. Although thermally-forced circulations have been studied extensively in the past, recently much attention has been focused on the scale of forcing (Xian and Pielke, 1991; Pielke et al., 1990), subgrid-scale parameterization (Avissar and Pielke, 1989; Dalu et al., 1991a, b; Pielke et al., 1991a), surface and subsurface parameterization (Lee et al., 1992; Lee and Pielke, 1992), and coupled ecosystem-atmosphere modeling (Lee and Pielke, 1991; Lee, 1992; Pielke et al., 1991a, 1992). It has been hypothesized that the change of land-use and landscape patterns over the world may have already altered the climate as much as the hypothesized greenhouse effect.

The impact of landscape and land-use (i.e., variable surface characteristics) on generating

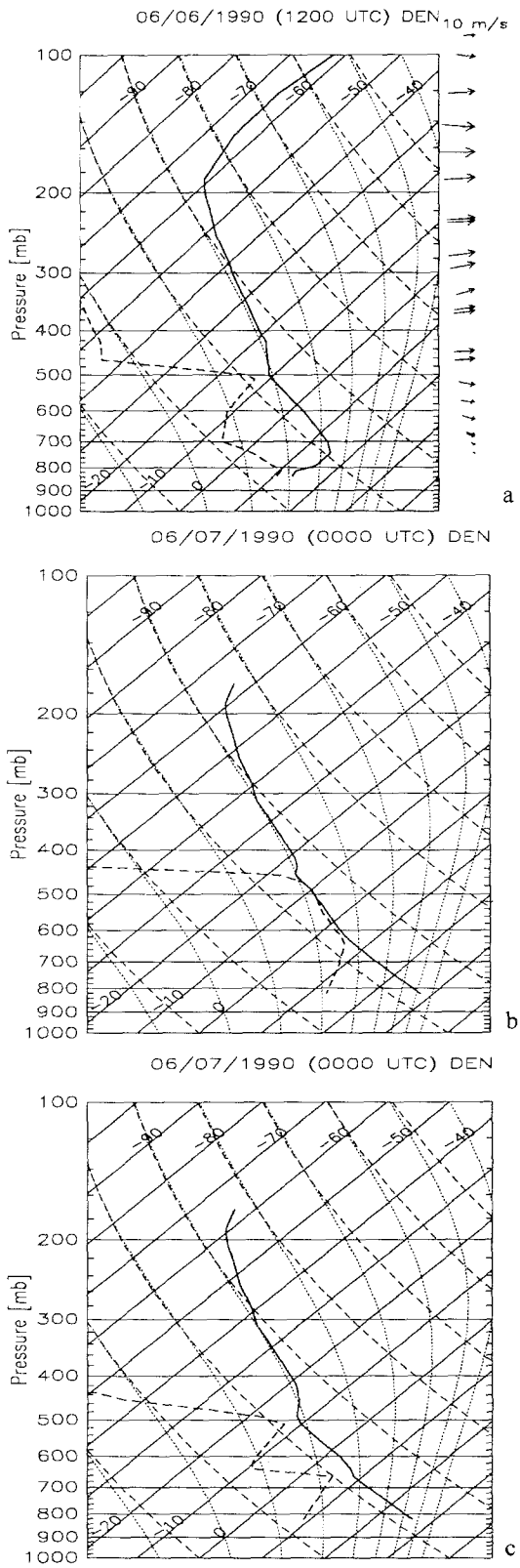


Fig. 16. One-dimensional sensitivity study with different surface characteristics. The model was initialized with a Denver morning sounding shown in panel (a). Panels (b) and (c) show the simulated afternoon sounding with and without vegetation cover, respectively (from Lee and Pielke, 1991)

thermally-direct atmospheric circulations has been studied using RAMS. Using the RAMS surface submodel (Land Ecosystem-Atmospheric Feedback Model-LEAF), which is described in Lee et al. (1992), sensitivity studies have been performed which show that the presence of vegetation can alter atmospheric boundary layer structure (Segal et al., 1988a), enrich the moist static energy in the atmospheric boundary layer (Pielke and Zeng, 1989), and trigger and enhance deep cumulus convection (Lee and Pielke, 1991). Figure 16 shows a one-dimensional sensitivity analysis of two simulations, one with and one without the existence of vegetation. It clearly shows that a cloudy layer can form at the top of the atmospheric boundary layer simply due to the enrichment of atmospheric boundary layer moisture when vegetation exists. When this vegetated surface is juxtaposed to dry land, the simulated circulation pattern and the circulation intensity (Pielke et al., 1990) are quite similar to a sea-breeze circulation. Since sea-breeze convergence can generate deep cumulonimbus convection, similar results are likely to occur due to landscape variability. The resulting increase in convective precipitation frequency may change the surface characteristics in the long run, contributing to a change in local vegetation type.

## 10. Application of RAMS to Atmospheric Dispersion Modeling

Since physiographic forcing can add considerable complexity to mesoscale flow fields, "mean" wind fields over land will normally be nonstationary and inhomogeneous on the mesoscale. Even over flat, homogeneous terrain, there are two natural mesoscale time scales: the diurnal period and the inertial period (McNider et al., 1988; Moran et al., 1991). This mesoscale variability poses considerable difficulties for air quality modelers wishing to simulate atmospheric dispersion on the mesoscale since the simplest types of dispersion models (Gaussian puff and plume models; similarity theory models) assume the background flow to be both stationary and homogeneous (e.g., Pielke et al., 1991b). More complex air quality models have been devised to simulate long-range transport of air pollutants, but most of these larger-scale dispersion models employ so-called diagnostic wind-field models to specify the transport wind field. The latter "models" are basically objective-analysis schemes for wind observations and hence are limited by the temporal and spatial resolution of the operational synoptic-scale observing network (e.g., Draxler, 1987; Venkatram et al., 1988; Moran et al., 1991).

Such observational limitations can be avoided, or at least minimized, if a prognostic meteorological model such as RAMS is coupled to an air quality model: the meteorological model is used to predict the time-dependent, three-dimensional dynamic and thermodynamic meteorological fields and the air quality model then takes these fields as inputs and calculates the resulting atmospheric transport and diffusion for a specified pollutant source or sources. Wind observations, if available, can be incorporated into the prognosed wind fields through the use of various 4DDA techniques.

RAMS has been used in conjunction with a mesoscale Lagrangian particle dispersion model, or MLPDM, to study mesoscale atmospheric dispersion in a variety of situations. This MLPDM was originally developed by McNider (McNider, 1981; McNider et al., 1980, 1982). Turbulent dispersion is modeled by simulating the simultaneous or sequential release of a large number of passive pollutant point-particles and then advecting these particles in response to the resolved mean flow field predicted by RAMS and to parameterized random turbulent fluctuations calculated from other RAMS atmospheric and surface fields. Concentration field moments can then be estimated

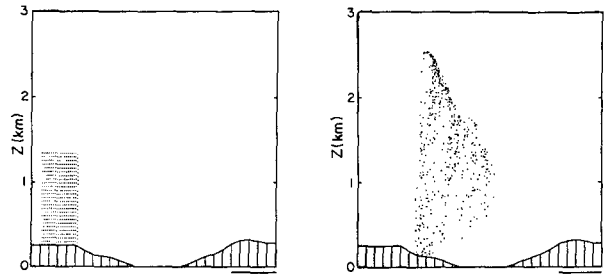


Fig. 17. Vertical cross section, looking eastward, showing the transport and turbulent diffusion of 500 particles being carried southward across Lake Ontario by a 2.5 $ms^{-1}$ synoptic wind on an early summer day: (a) 0815 Local Solar Time [and time of release]; (b) 1715 LST. The meteorological model domain was two-dimensional, horizontal grid interval was 10 km, and the domain depth was 6 km with 22 vertical levels. Lake Ontario is the flat sunken region in the center of the figure; lake surface temperature was taken to be uniform and equal to 10 °C (from Moran et al., 1986)

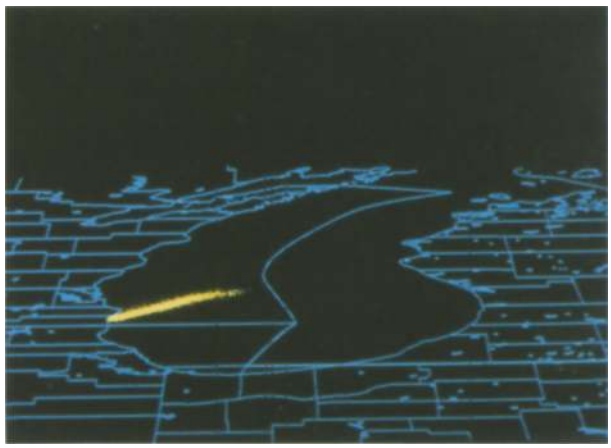

a

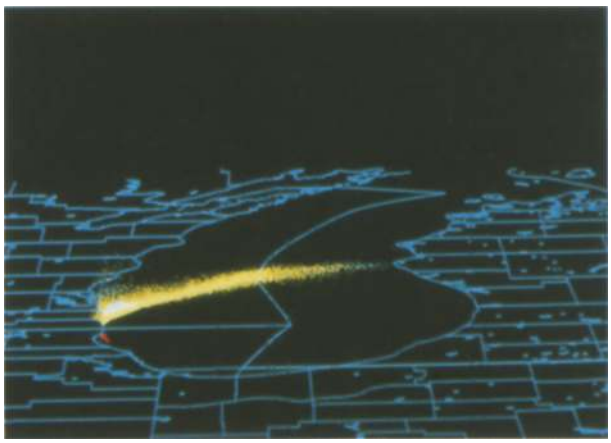

b

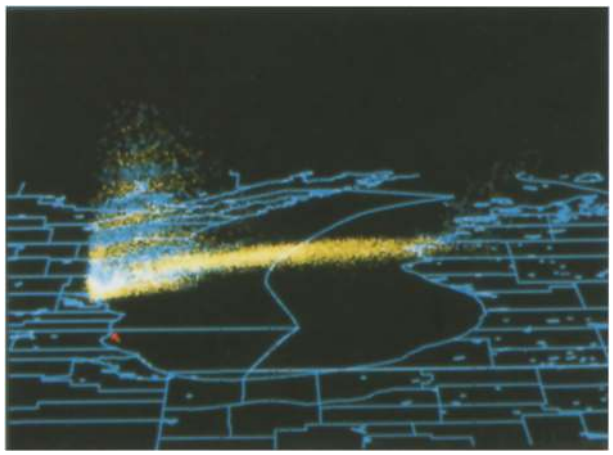

c

based on the spatial distribution of the set of predicted particle positions through estimation of the univariate or multivariate particle position probability density function $P(z, t)$. More details may be found in Pielke et al. (1983), Pielke (1984), McNider et al. (1988), and Pielke et al. (1991b). Currently, the Lagrangian particle model reported in Uliasz (1993) is being incorporated into RAMS.

Figure 17 shows results from an application of RAMS and the MLPDM to study the influence of a lake-breeze circulation on regional air pollution transport. The first panel shows the initial distribution of the point-particles in the morning on the left shore of the 50 km-wide lake. Flow at this site consists of a combination of light and steady left-to-right synoptic flow and a nascent onshore lake-breeze circulation. The second panel shows the subsequent particle distribution in the late afternoon. The particles on the left shore have been mixed through a deeper layer both by the growth of the daytime convective mixed layer over land and by "mesoscale venting" as the lake-breeze front advanced inland. The clear zone beneath the leading edge of the particle envelope over the lake suggests some recirculation of particles onshore in the lake breeze, counter to the prevailing synoptic flow, and also resistance to downward transport to the lake surface due to the low-level stable layer of air above the cold lake.

Figure 18 shows an MLPDM simulation of the complexities of mesoscale transport of a gaseous plume from a hypothetical nuclear plant on the western shore of Lake Michigan (Lyons et al., 1991b). The plume is emitted into a land/lake breeze circulation, beginning at 0530 LST and continuing for four hours. The plume initially advects northeastward over the cold lake. By mid-morning, a lake-breeze inflow develops along the western shore which re-entrains part of the plume landwards. By mid-day, the leading edge of the

Fig. 18. RAMS and MLPDM simulation of a four-hour release of a plume into a land/lake breeze from a hypothetical accident at a nuclear plant located on the western shoreline of Lake Michigan. The plume was released at 50 m height beginning at 0530 LST. The plume is shown (top) after 2.5 hours of transport over water, (middle) at 1100 LST, some 90 minutes after the end of the release, and (bottom) at 1400 LST as the distorted plume continues to be transported over the lake and along both shores. Visualization prepared with SSESCO's savi3D software, courtesy of Neil Lincoln and Dennis Moon of Minneapolis, Minnesota

plume is crossing the eastern shoreline, mixing upward in the thermal internal boundary layer there. Minimal vertical mixing is present over the lake. Along the western shore, plume matter is involved in the complex lake-breeze frontal dynamics, with individual trajectories resembling along-shore helical vortices.

Other applications of this mesoscale dispersion modeling system to date include (a) idealized studies of mesoscale influences on long-range transport (Moran et al., 1986; McNider et al., 1988; Segal et al., 1988b, d; Pielke et al., 1991b), (b) air pollution impact studies for U.S. national parks (Segal et al., 1988c, d; Pielke et al., 1991b) and other areas of complex terrain (Yu and Pielke, 1986; Pielke et al., 1987a; Lyons et al., 1991a), (c) mesoscale tracer experiment simulations (Pielke et al., 1991b; Moran, 1992), and (d) emergency response dispersion forecasting (Pielke et al., 1987b; Lyons et al., 1991b).

## 11. Computer Capabilities

About five years ago, people would make comments such as "Someday we will all have computers as fast as a Cray-1 on our desks." Another comment of that time was "Yes, we will have a Cray-1 on our desks, but the rest of the desk will be a cooling system!" The actual forecast was that maybe by the mid-1990s, small computers would attain that speed and capacity of the large supercomputers of the 1980s. By 1990, due to unprecedented advances in computer hardware, Reduced Instruction Set Computers (RISC)-based workstations from many manufacturers (IBM, Hewlett-Packard, Stardent, SUN, etc.) have met and exceeded the capabilities of a single Cray-1 processor.

RAMS, like all large scientific codes, had historically been targeted for the large main-frame supercomputer. There were no other machines available that would be feasible to run the large codes. Starting from its predecessors in the mid-1970's, RAMS has been structured to take advantage of the vector processing architectures of the big machines. Now, with the advent of the fast RISC workstations, more machines exist so that the requirement of portability of the RAMS code is a much more important issue. RAMS has been executed on a wide variety of platforms including the Cray's, Cyber 205, ETA, and NEC machines. In addition to the traditional supercomputers, RAMS has been run on machines as far-ranging as DEC VAX's, IBM 3090, IBM RS/6000, Apollo, Hewlett-Packard, Sun, Stardent, Silicon Graphics, Convex, and even a Compaq 386 PC.

Although there exist a wide range of model configurations which will affect the details of the computer configuration necessary to execute RAMS, a few guidelines can be mentioned. To be able to execute an average-size three-dimensional simulation (about 64,000 grid points) in a reasonable amount of time, the computer should have 8 million words (32 Mbytes on a 32-bit machine), about 1 Gbyte of disk space, and perform 10 or more Mflops on the standard LINPACK benchmark. The actual execution time for any run is dependent on the actual options chosen. For smaller or larger simulations, this configuration can be adjusted accordingly. RAMS does not rely on any of the mathematical libraries such as IMSL. It only requires a FORTRAN compiler (although a few C routines will be used in the future).

Scientific visualization is another area where the RISC workstations have allowed important advancements over the last few years. In the past, vector graphics packages (NCAR Graphics, DISSPLA, etc.) were used to display results from scientific codes. The output from these packages were mostly monochrome, two-dimensional depictions of the model results; for instance, a contour plot. The standard visualization output from RAMS is still produced with NCAR Graphics. Now with the RISC workstations and new visualization tools such as AVS from Stardent and GL from Silicon Graphics, color displays, three-dimensional volume renderings, and color animations of the model results are becoming possible.

As the computer hardware and software continue their evolutionary advances, RAMS will also change to take advantage of the new technologies. There are two main changes that will occur in the RAMS software in the near-term:

- The parallelization of the code has been started. We are considering both the shared and distributed memory architectures when restructuring the code. Prototype versions of RAMS have been executed on the CM-2 machine and a RISC workstation cluster.
- Standardization of a new visualization interface for the model results, data analysis, and user input. An interface using Stardent's AVS package is underway.

## 12. Summary

This paper has surveyed a range of applications of the Regional Atmospheric Modeling System (RAMS). Applications discussed in this paper include large eddy simulations (LES), thunderstorms, cumulus fields, mesoscale convective systems, mid-latitude cirrus clouds, winter storms, mechanically- and thermally-forced mesoscale systems, and mesoscale atmospheric dispersion. A summary of current RAMS options was also presented. Improvements to RAMS currently underway include refinements to the cloud radiation, cloud microphysics, cumulus, and surface soil/vegetative parameterization schemes, the parallelization of the code, development of a more versatile visualization capability, and research into meso-$\alpha$-scale cumulus parameterizations.

### Acknowledgments

The work reported in this paper was supported by the National Science Foundation under grant #ATM-8915265 and #ATM-8814913, Army Research Office under contract #DAAL03-86-K-0175, Air Force Office of Scientific Research under contract #AFOSR-91-0269. The editorial preparation of the paper was ably completed by Dallas McDonald and Bryan Critchfield. Several of the model calculations reported on in this paper were completed at the National Center for Atmospheric Research (NCAR). NCAR is partially supported by National Science Foundation. The other model calculations were completed on IBM RISC 6000 model 550 and 320 H high performance workstations, and on a Stardent superminicomputer.

### References

Atwater, M. A., Brown, Jr., P. S., 1974: Numerical calculation of the latitudinal variation of solar radiation for an atmosphere of varying opacity. *J. Appl. Meteor.*, **13**, 289–297.

Avissar, R., Mahrer, Y., 1988: Mapping frost-sensitive areas with a three-dimensional local-scale numerical model. Part I: Physical and numerical aspects. *J. Appl. Meteor.*, **27**, 400–413.

Avissar, R., Pielke, R. A., 1989: A parameterization of heterogeneous land surfaces for atmospheric numerical models and its impact on regional meteorology. *Mon. Wea. Rev.*, **117**, 2113–2136.

Barnes, S. L., 1973: Mesoscale objective map analysis using weighted time-series observations. NOAA Tech. Memo. ERL NSSL-62 [NTIS COM-73-10781], March, National Severe Storms Laboratory, Norman, Oklahoma, 60 pp.

Bleck, R., Haagenson, P. L., 1968: Objective analysis on isentropic surfaces. NCAR Tech. Note, TN-39, December, National Center for Atmospheric Research, Boulder, Colorado, 27 pp.

Bossert, J. E., 1990: Regional-scale flows in complex terrain: an observational and numerical investigation. Paper No. 472, Department of Atmospheric Science, Colorado State University, Fort Collins, Colorado, 254 pp.

Buckley, A., 1985: Algorithm 630: BBVSCG – a variable-storage algorithm for function minimization. *ACM Trans. on Math. Soft.*, **11**, 103–119.

Chen, C., Cotton, W. R., 1983: A one-dimensional simulation of the stratocumulus-capped mixed layer. *Bound.-Layer Meteor.*, **25**, 289–321.

Chen, C., Cotton, W. R., 1987: The physics of the marine stratocumulus-capped mixed layer. *J. Atmos. Sci.*, **44**, 2951–2977.

Chen, S., Cotton, W. R., 1988: The sensitivity of a simulated extratropical mesoscale convective system to longwave radiation and ice-phase microphysics. *J. Atmos. Sci.*, **45**, 3897–3910.

Clark, T. L., Farley, R. D., 1984: Severe downslope windstorm calculations in two and three spatial dimensions using anelastic interactive grid nesting: A possible mechanism for gustiness. *J. Atmos. Sci.*, **41**, 329–350.

Copeland, J. H., Pielke, R. A., Cotton, W. R., 1991: The effect of four-dimensional data density on assimilation for a shallow-water model with the adjoint method: Preliminary results. *Proceedings, Ninth AMS Conference on Numerical Weather Prediction*, October 14–18, Denver, Colorado, Amer. Meteor. Soc., Boston, 183–185.

Cotton, W. R., 1991: Numerical simulations of tornadic-producing storms and tornado vortices. Final Report to NOAA/ERL, Norman, OK, Contract #NA85RAH0545, Item 24, AMD 29, 15 pp. [Available from W. R. Cotton].

Cotton, W. R., Stephens, M. A., Nehrkorn, T., Tripoli, G. J., 1982: The Colorado State University three-dimensional cloud/mesoscale model – 1982. Part II: An ice phase parameterization. *J. de Rech. Atmos.*, **16**, 295–320.

Cotton, W. R., Tripoli, G. J., Rauber, R. M., Mulvihill, E. A., 1986: Numerical simulation of the effects of varying ice crystal nucleation rates and aggregation processes on orographic snowfall. *J. Climate Appl. Meteor.*, **25**, 1658–1680.

Courtier, P., Talagrand, O., 1990: Variational assimilation of meteorological observations with the direct and adjoint shallow-water equations. *Tellus*, **42A**, 531–549.

Cram, J. M., 1990: Numerical simulation and analysis of the propagation of a prefrontal squall line. Ph.D. dissertation, Dept. of Atmospheric Science, Colorado State University, Ft. Collins, CO, 330 pp.

Cram, J. M., Pielke, R. A., Cotton, W. R., 1992a: Numerical simulation and analysis of a prefrontal squall line. Part I: Observations and basic simulation results. *J. Atmos. Sci.*, **49**, 189–208.

Cram, J. M., Pielke, R. A., Cotton, W. R., 1992b: Numerical simulation and analysis of a prefrontal squall line. Part II: Propagation of the squall line as an internal gravity wave. *J. Atmos. Sci.*, **49**, 209–228.

Dalu, G. A., Baldi, M., Pielke, R. A., Lee, T. J., Colacino, M., 1991a: Mesoscale vertical velocities generated by stress changes in the boundary layer: Linear theory. *Ann. Geophys.* (in press).

Dalu, G. A., Pielke, R. A., Avissar, R., Kallos, G., Baldi, M., Guerrini, A., 1991b: Linear impact of thermal inhomogeneities on mesoscale atmospheric flow with zero synoptic wind. *Ann. Geophys.* **9**, 641–647.

Davies, H. C., 1983: Limitations of some common lateral

boundary schemes used in regional NWP models. *Mon. Wea. Rev.*, **111**, 1002–1012.

Deardorff, J. W., 1980: Stratocumulus-capped mixed layers derived from a three-dimensional model. *Bound.-Layer Meteor.*, **18**, 495–527.

Draxler, R. R., 1987: Sensitivity of a trajectory model to the spatial and temporal resolution of the meteorological data during CAPTEX. *J. Climate Appl. Meteor.*, **26**, 1577–1588.

Garratt, J. R., Brost, R. A., 1981: Radiative cooling effects within and above the nocturnal boundary layer. *J. Atmos. Sci.*, **38**, 2730–2746.

Goodchild, M. F., Parks, B., Steyaert, L. T. (eds.) 1992: *Integrating Geographic Information Systems and Environmental Modeling*, Oxford Press (in press).

Grasso, L. D., 1992: Tornadogenesis. M.S. Thesis, Department of Atmospheric Science, Colorado State University, Fort Collins, Colorado, 102 pp.

Hadfield, M. G., Cotton, W. R., Pielke, R. A., 1991: Large-eddy simulations of thermally-forced circulations in the convective boundary layer. Part I: A small-scale circulation with zero wind. *Bound.-Layer Meteor.*, **57**, 79–114.

Heckman, S. T., 1991: Numerical simulation of cirrus clouds – FIRE case study and sensitivity analysis. M.S. Thesis (and Atmospheric Science Paper #483), Department of Atmospheric Science, Colorado State University, Fort Collins, CO 80523, 132 pp.

Herman, G., Goody, R., 1976: Formation and persistence of summertime arctic stratus clouds. *J. Atmos. Sci.*, **33**, 1537–1553.

Jacobs, C. A., Pandolfo, J. P., Atwater, M. A., 1974: A description of a general three dimensional numerical simulation model of a coupled air-water and/or air-land boundary layer. IFYGL final report, CEM Report No. 5131-509a, The Center for the Environment and Man, Hartford, Connecticut.

Klemp, J. B., Durran, D. R., 1983: An upper boundary condition permitting internal gravity wave radiation in numerical mesoscale models. *Mon. Wea. Rev.*, **111**, 430–444.

Klemp, J. B., Lilly, D. K., 1978: Numerical simulation of hydrostatic mountain waves. *J. Atmos. Sci.*, **35**, 78–107.

Klemp, J. B., Wilhelmson, R. B., 1978a: The simulation of three-dimensional convective storm dynamics. *J. Atmos. Sci.*, **35**, 1070–1096.

Klemp, J. B., Wilhelmson, R. B., 1978b: Simulations of right- and left-moving storms produced through storm splitting. *J. Atmos, Sci.*, **35**, 1097–1110.

Kondrat'yev, J., 1969: *Radiation in the Atmosphere*. New York: Academic Press, 912 pp.

Lacis, A. A., Hansen, J., 1974: A parameterization for the absorption of solar radiation in earth's atmosphere. *J. Atmos. Sci.*, **31**, 118–133.

Lee, T. J., 1992: The impact of vegetation on the atmospheric boundary layer and convective storms. Ph.D. Dissertation, Department of Atmospheric Science, Colorado State University, Fort Collins, Colorado, 137 pp.

Lee, T. J., Pielke, R. A., 1992: Estimating the soil surface specific humidity. *J. Appl. Meteor.*, **31**, 480–484.

Lee, T. J., Pielke, R. A., 1991: The impact of vegetation on severe convective storms. *Proceedings, Ninth AMS Conference on Numerical Weather Prediction*, October 14–18, Denver, Colorado, Amer. Meteor. Soc., Boston, 242–244.

Lee, T. J., Pielke, R. A., Kessler, R. C., Weaver, J., 1989: Influence of cold pools down-stream of mountain barriers on downslope winds and flushing. *Mon. Wea. Rev.*, **117**, 2041–2058.

Lee, T. J., Pielke, R. A., Kittel, T. G. F., Weaver, J. F., 1992: Atmospheric modeling and its spatial representation of land surface characteristics. In: Goodchild, M. F., Parks, B., Steyaert, L. T. (eds.) *Integrating Geographic Information Systems and Environmental Modeling*. Oxford University Press (in press).

Lewis, J., Derber, J., 1985: The use of adjoint equations to solve a variational adjustment problem with advective constraints. *Tellus*, **37A**, 309–322.

Louis, J. F., 1979: A parametric model of vertical eddy fluxes in the atmosphere. *Bound.-Layer Meteor.*, **17**, 187–202.

Lyons, W. A., Pielke, R. A., Eastman, J. L., Moon, D. A., Keen, C. S., Lincoln, N. R., 1991a: Mesoscale numerical model evaluations of the meteorological factors associated with elevated ozone levels in the southern Lake Michigan region. *Proc. Seventh AMS/AWMA Joint Conference on Applications of Air Pollution Meteorology*, January 13–18, New Orleans, Amer. Meteor. Soc., Boston, 164–167.

Lyons, W. A., Moon, D. A., Venne, M. G., Keen, C. S., Lincoln, N. R., Pielke, R. A., Cotton, W. R., Tremback, C. J., Walko, R. L., 1991b: Real-time forecasting of the impacts of accidental releases of radionuclides into complex coastal zone mesoscale regimes using the Advanced Regional Atmospheric Modeling System (ARAMS). *Proc. Seventh Joint AMS/AWMA Conference on Applications of Air Pollution Meteorology*, January 14–18, New Orleans, Amer. Meteor. Soc., Boston, 205–208.

Lyons, W. A., Walko, R. L., Nicholls, M. E., Pielke, R. A., Cotton, W. R., Keen, C. S., Watson, A. I., 1992: Observational and numerical modeling investigations of Florida thunderstorms generated by multi-scale surface thermal forcing. *Proc. Fifth AMS Conference on Mesoscale Processes, January* 5–10, Atlanta, GA, Amer. Meteor. Soc., Boston, 85–90 pp.

Mahrer, Y., Pielke, R. A., 1977: A numerical study of the airflow over irregular terrain. *Beiträge zur Physik der Atmosphäre*, **50**, 98–113.

McCumber, M. D., 1980: A numerical simulation of the influence of heat and moisture fluxes upon mesoscale circulation. Ph.D. dissertation, Dept. of Environmental Science, University of Virginia, Charlottesville, Virginia, 225 pp.

McCumber, M. C., Pielke, R. A., 1981: Simulation of the effects of surface fluxes of heat and moisture in a mesoscale numerical model. Part I: Soil layer. *J. Geophys. Res.*, **86**, 9929–9938.

McDonald, J. E., 1960: Direct absorption of solar radiation by atmospheric water vapor. *J. Meteor.*, **17**, 319–328.

McNider, R. T., 1981: Investigation of the impact of topographic circulations on the transport and dispersion of air pollutants. Ph.D. Dissertation, University of Virginia, Charlottesville, Virginia, 210 pp.

McNider, R. T., Pielke, R. A., 1981: Diurnal boundary-layer development over sloping terrain. *J. Atmos. Sci.*, **38**, 2198–2212.

McNider, R. T., Hanna, S. R., Pielke, R. A., 1980: Sub-grid scale plume dispersion in coarse resolution mesoscale models. *Proc. Second Joint AMS/APCA Conference on Applications of Air Pollution Meteorology*, March 24–27, New Orleans, Amer. Meteor. Soc., Boston, 424–429.

McNider, R. T., Anderson, K. J., Pielke, R. A., 1982: Numerical simulation of plume impaction. *Proc. Third Joint AMS/APCA Conference on Applications of Air Pollution Meteorology*, January 12–15, San Antonio, Amer. Meteor. Soc., Boston, 126–129.

McNider, R. T., Moran, M. D., Pielke, R. A., 1988: Influence of diurnal and inertial boundary layer oscillations on long-range dispersion. *Atmos. Environ.*, **22**, 2445–2462.

Mellor, G. L., Yamada, T., 1982: Development of a turbulence closure model for geophysical fluid problems. *Rev. Geophys. Space Phys.*, **20**, 851–875.

Meyers, M. P., Cotton, W. R., 1992: Evaluation of the potential for wintertime quantitative precipitation forecasting over mountainous terrain with an explicit cloud model. Part I: Two-dimensional sensitivity experiments. *J. Appl. Meteor.*, **31**, 26–50.

Meyers, M. P., DeMott, P. J., Cotton, W. R., 1992: New primary ice nucleation parameterizations in an explicit cloud model. *J. Appl. Meteor.*, **31**, 708–721.

Moeng, C.-H., Wyngaard, J. C., 1984: Statistics of conservative scalars in the convective boundary layer. *J. Atmos. Sci.*, **41**, 2052–2062.

Moran, M. D., 1992: Numerical modeling of mesoscale atmospheric dispersion. Ph.D. dissertation, Department of Atmospheric Science, Colorado State University, Fort Collins, Colorado, 820 pp.

Moran, M. D., Arritt, R. W., Segal, M., Pielke, R. A., 1986: Modification of regional-scale pollutant dispersion by terrain-forced mesoscale circulations. *Transactions, APCA Second International Specialty Conference on the Meteorology of Acidic Deposition*, March, 17–20, Albany, New York, Air Pollution Control Association, Pittsburgh, Pennsylvania, 136–157.

Moran, M. D., Pielke, R. A., McNider, R. T., 1991: Temporal and spatial resolution requirements for regional-scale dispersion models. In: van Dop, H., Steyn, D. G. (eds.) *Air Pollution Modeling and its Application VIII*. New York: Plenum Press, 427–437.

Nicholls, M. E., Johnson, R. H., Cotton, W. R., 1988: The sensitivity of two-dimensional simulations of tropical squall lines to environmental profiles. *J. Atmos. Sci.*, **45**, 3625–3649.

Nicholls, M. E., Pielke, R. A., Cotton, W. R., 1991: A two-dimensional numerical investigation of the interaction between sea-breezes and deep convection over the Florida peninsula. *Mon. Wea. Rev.*, **119**, 298–323.

Orlanski, I., 1976: A simple boundary condition for unbounded hyperbolic flows. *J. Comput. Phys.*, **21**, 251–269.

Perkey, D. J., Kreitzberg, C. W., 1976: A time-dependent lateral boundary scheme for limited-area primitive equation models. *Mon. Wea. Rev.*, **104**, 744–755.

Pielke, R. A., 1984: Mesoscale Meteorological Modeling. New York, N.Y.: Academic Press, 612 pp.

Pielke, R. A., Arritt, R. W., 1984: A proposal to standardize models. *Bull. Amer. Meteor. Soc.*, **65**, 1082.

Pielke, R. A., Zeng, X., 1989: Influence on severe storm development of irrigated land. *Natl. Wea. Dig.*, **14**, 16–17.

Pielke, R. A., McNider, R. T., Segal, M., Mahrer, Y., 1983: The use of a mesoscale numerical model for evaluations of pollutant transport and diffusion in coastal regions and over irregular terrain. *Bull. Amer. Meteor. Soc.*, **64**, 243–249.

Pielke, R. A., Arritt, R. W., Segal, M., Moran, M. D., McNider, R. T., 1987a: Mesoscale numerical modeling of pollutant transport in complex terrin. *Bound.-Layer Meteor.*, **41**, 59–74.

Pielke, R. A., Moran, M. D., Segal, M., Wesley, D. A., McKee, T. B., 1987b: Opportunities for nowcasting air pollution episodes and accidental toxic and radioactive releases. *Proc. IUGG Symposium on Mesoscale Analysis and Forecasting, Incorporating Nowcasting*, August 17–19, Vancouver, British Columbia, Canada, International Union of Geodesy and Geophysics, Geneva, 463–470.

Pielke, R. A., Lee, T. J., Weaver, J., Kittel, T. G. F., 1990: Influence of vegetation on the water and heat distribution over mesoscale sized areas. *Preprints, 8th AMS Conference on Hydrometeorology*, October 22–26, Kananaskis Provincial Park, Alberta, Canada, Amer. Meteor. Soc., Boston, 46–49.

Pielke, R. A., Dalu, G., Snook, J. S., Lee, T. J., Kittel, T. G. F., 1991a: Nonlinear influence of mesoscale landuse on weather and climate. *J. Climate*, **4**, 1053–1069.

Pielke, R. A., Lyons, W. A., McNider, R. T., Moran, M. D., Moon, D. A., Stocker, R. A., Walko, R. L., Uliasz, M., 1991b: Regional and mesoscale meteorological modeling as applied to air quality studies. In: van Dop, H., Steyn D. G. (eds.) *Air Pollution Modeling and its Application VIII*. New York: Plenum Press, 259–289.

Pielke, R. A., Schimel, D. S., Lee, T. J., Kittel, T. G. F., Zeng, X., 1992: Atmosphere-terrestrial ecosystem interactions: Implications for coupled modeling. *Ecological Modelling* (in press).

Rasmussen, R. M., Politovich, M. K., 1990: WISP Scientific Overview. NCAR publication available from authors, National Center for Atmospheric Research, P.O. Box 3000, Boulder, CO 80307.

Rodgers, C. D., 1967: The use of emissivity in atmospheric radiation calculations. *Quart. J. Roy. Meteor. Soc.*, **93**, 43–54.

Sasamori, T., 1972: A linear harmonic analysis of atmospheric motion with radiative dissipation. *J. Meteor. Soc. Japan*, **50**, 505–518.

Schmidt, J. M., 1991: Numerical and observational investigations of long-lived, MCS-induced, severe surface wind events: The derecho. Ph.D. Dissertation, Department of Atmospheric Science, Colorado State University, Fort Collins, CO 80523, 196 pp.

Schmidt, J. M., Cotton, W. R., 1990: Interactions between upper and lower tropospheric gravity waves on squall line structure and maintenance. *J. Atmos. Sci.*, **47**, 1205–1222.

Segal, M., Avissar, R., McCumber, M. C., Pielke, R. A., 1988a: Evaluation of vegetation effects on the generation and

modification of mesoscale circulations. *J. Atmos. Sci.*, **45**, 2268–2292.

Segal, M., Yu, C.-H., Arritt, R. W., Pielke, R. A., 1988b: On the impact of valley/ridge thermally induced circulations on regional pollutant transport. *Atmos. Environ.*, **22**, 471–486.

Segal, M., Pielke, R. A., Arritt, R. W., Moran, M. D., Yu, C.-H., Henderson, D., 1988c: Application of a mesoscale atmospheric dispersion modeling system to the estimation of $SO_2$ concentrations from major elevated sources in southern Florida. *Atmos. Environ.*, **22**, 1319–1334.

Segal, M., Yu, C.-H., Pielke, R. A., 1988d: Model evaluation of the impact of thermally-induced valley circulations in the Lake Powell area on long-range pollutant transport. *J. Air Poll. Control Assoc.*, **38**, 163–170.

Stauffer, D. R., Seaman, N. L., 1990: Use of four-dimensional data assimilation in a limited-area mesoscale model. Part I: Experiments with synoptic-scale data. *Mon. Wea. Rev.*, **118**, 1250–1277.

Stephens, G. L., 1977: The transfer of radiation in cloudy atmosphere. Ph.D. dissertation. Meteorology Department, University of Melbourne, Australia, 396 pp.

Stephens, G. L., 1978: Radiation profiles in extended water clouds. Theory. *J. Atmos. Sci.*, **35**, 2111–2122.

Talagrand, O., Courtier, P., 1987: Variational assimilation of meteorological observations with the adjoint vorticity equation – Part I. Theory. *Quart. J. Roy. Meteor. Soc.*, **113**, 1311–1328.

Taylor, G., 1991: Data assimilation and the adjoint method: An overview. CIRA-USARO Rep. No. 0737-5352-22, Cooperative Institute for Research in the Atmosphere, Colorado State University, Fort Collins, 13 pp.

Thacker, W., Long, R., 1988: Fitting dynamics to data. *J. Geophys. Res.*, **93**, 1227–1240.

Tremback, C. J., 1990: Numerical simulation of a mesoscale convective complex: model development and numerical results. Ph.D. dissertation, Atmos. Sci. Paper No. 465, Department of Atmospheric Science, Colorado State University, Fort Collins, CO 80523, 247 pp.

Tremback, C. J., Kessler, R., 1985: A surface temperature and moisture parameterization for use in mesoscale numerical models. *Preprints, 7th AMS Conference on Numerical Weather Prediction*, June 17–20, Montreal, Quebec, Canada, Amer. Meteor. Soc., Boston, 355–358.

Tremback, C. J., Tripoli, G. J., Cotton, W. R., 1985: A regional scale atmospheric numerical model including explicit moist physics and a hydrostatic time-split scheme. *Preprints, 7th AMS Conference on Numerical Weather Prediction*, June 17–20, Montreal, Quebec, Canada, Amer. Meteor. Soc., Boston, 433–434.

Tremback, C. J., Powell, J., Cotton, W. R., Pielke, R. A., 1987: The forward-in-time upstream advection scheme: Extension to higher orders. *Mon. Wea. Rev.*, **115**, 540–555.

Tripoli, G. J., Cotton, W. R., 1980: A numerical investigation of several factors contributing to the observed variable intensity of deep convection over south Florida. *J. Appl. Meteor.*, **19**, 1037–1063.

Tripoli, G. J., Cotton, W. R., 1982: The Colorado State University three-dimensional cloud/mesoscale model – 1982. Part I: General theoretical framework and sensitivity experiments. *J. de Rech. Atmos.*, **16**, 185–220.

Tripoli, G. J., Cotton, W. R., 1986: An intense, quasi-steady thunderstorm over mountainous terrain Part IV: Three-dimensional numerical simulation. *J. Atmos. Sci.*, **43**, 896–914.

Tripoli, G., Cotton, W. R., 1989a: A numerical study of an observed orogenic mesoscale convective system. Part 1: Simulated genesis and comparison with observations. *Mon. Wea. Rev.*, **117**, 273–304.

Tripoli, G., Cotton, W. R., 1989b: A numerical study of an observed orogenic mesoscale convective system. Part 2: Analysis of governing dynamics. *Mon. Wea. Rev.*, **117**, 305–328.

Uliasz, M., 1993: Atmospheric mesoscale dispersion modeling system – MDMS. *J. Appl. Meteor.* (in press).

Venkatram, A., Karamchandani, P. K., Misra, P. K., 1988: Testing a comprehensive acid deposition model. *Atmos. Environ.*, **22**, 737–747.

Verlinde, J., 1992: Fitting microphysical observations to a numerical model through an optimal control theory technique. Ph.D. dissertation (and Atmospheric Science Paper No. 493), Department of Atmospheric Science, Colorado State University, Fort Collins, Colorado 80523, 83 pp.

Walko, R. L., Tremback, C. J., 1991: RAMS – The Regional Atmospheric Modeling System Version 2C: User's guide. Published by ASTeR, Inc., P.O. Box 466, Fort Collins, Colorado, 86 pp.

Walko, R. L., Tremback, C. J., Cotton, W. R., 1989: Assimilation of Doppler radar wind data into a numerical prediction model: A demonstration of certain hazards. *Preprints, 24th AMS Conference on Radar Meteorology*, March 27–31, Tallahassee, Florida, Amer. Meteor. Soc., Boston, 248–250 pp.

Walko, R. L., Cotton, W. R., Pielke, R. A., 1992: Large eddy simulation of the effects of hilly terrain on the convective boundary layer. *Bound.-Layer Meteor.*, **58**, 133–150.

Wang, W., Warner, T. T., 1988: Use of four-dimensional data assimilation by Newtonian relaxation and latent-heat forcing to improve a mesoscale-model precipitation forecast: A case study. *Mon. Wea. Rev.*, **116**, 2593–2613.

Weissbluth, M. J., 1991: Convective parameterization in mesoscale models. Ph.D. Dissertation, Department of Atmospheric Science, Colorado State University, Fort Collins, 211 pp.

Wesley, D. A., 1991: An investigation of the effects of topography on Colorado Front Range winter storms. Ph.D. Dissertation, Department of Atmospheric Science, Colorado State University, Fort Collins, Colorado, 197 pp.

Wesley, D. A., Pielke, R. A., 1990: Observations of blocking-induced convergence zones and effects on precipitation in complex terrain. *Atmos. Res.*, **25**, 235–276.

Wesley, D. A., Weaver, J. F., Pielke, R. A., 1990: Heavy snowfall during an extreme arctic outbreak along the Colorado Front Range. *Natl. Wea. Dig.*, **15**, 2–19.

Xian, Z., Pielke, R. A., 1991: The effects of width of land masses on the development of sea breezes. *J. Appl. Meteor.*, **30**, 1280–1304.

Yamamoto, G., 1962: Direct absorption of solar radiation by

atmospheric water vapor carbon dioxide and molecular oxygen. *J. Atmos. Sci.*, **19**, 182–188.

Yu, C.-H., Pielke, R. A., 1986: Mesoscale air quality under stagnant synoptic cold season conditions in the Lake Powell area. *Atmos. Environ.*, **20**, 1751–1762.

Authors' address: Dr. R. A. Pielke, W. R. Cotton, R. L. Walko, C. J. Tremback, W. A. Lyons, L. D. Grasso, M. E. Nicholls, M. D. Moran, D. A. Wesley, T. J. Lee and J. H. Copeland, Department of Atmospheric Science, Colorado State University, Fort Collins, CO 80523, U.S.A.